BIOCHEMISTRY
including biophysical chemistry & molecular biology

Article

pubs.acs.org/biochemistry

Second Double-Stranded RNA Binding Domain of Dicer-like Ribonuclease 1: Structural and Biochemical Characterization

Paula Burdisso,[†] Irina P. Suarez,[†] Nicolás G. Bologna,[†,⊥] Javier F. Palatnik,[†] Beate Bersch,[‡,§,∥] and Rodolfo M. Rasia*[,†]

[†]Instituto de Biología Molecular y Celular de Rosario (IBR-CONICET), Facultad de Ciencias Bioquímicas y Farmacéuticas, Universidad Nacional de Rosario, Santa Fe, Argentina

[‡]CNRS, Institut de Biologie Structurale Jean-Pierre Ebel, Grenoble, France

[§]CEA, IBS-Grenoble, Grenoble, France

[∥]Université de Grenoble 1, Grenoble, France

Supporting Information

ABSTRACT: Dicer-like ribonuclease III enzymes are involved in different paths related to RNA silencing in plants. Little is known about the structural aspects of these processes. Here we present a structural characterization of the second double-stranded RNA binding domain (dsRBD) of DCL1, which is presumed to participate in pri-micro-RNA recognition and subcellular localization of this protein. We determined the solution structure and found that it has a canonical fold but bears some variation with respect to other homologous domains. We also found that this domain binds both double-stranded RNA and double-stranded DNA, in contrast to most dsRBDs. Our characterization shows that this domain likely has functions other than substrate recognition and binding.

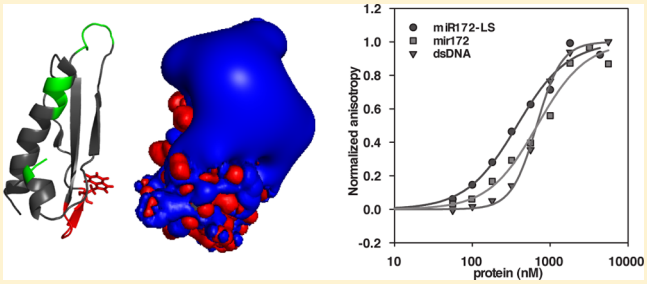

Micro-RNAs (miRNAs) make up a class of endogenous small RNAs that negatively regulate the expression of target mRNAs in higher organisms.[1] They originate in longer precursors (pri-miRNA) that present a hairpin structure and are transcribed by RNA polymerase II. The biogenesis of miRNAs is a complex process in which the structure of the precursor plays a key role in defining the final sequence of the mature miRNA.[2−5] In plants, pri-miRNAs are processed in the nucleus by a protein complex formed by DCL1, HYL1, and SERRATE that releases the miRNA−miRNA* duplex from the precursor.[6] These duplexes are then methylated by methyl-transferase HEN1 and transported to the cytoplasm, where they exert their regulatory role in the context of the RISC complex.[7]

The release of the miRNA from its precursor is performed by RNase III enzymes of the Dicer family. These enzymes have a conserved domain architecture, featuring one or two double-stranded RNA binding domains (dsRBDs) at the C-terminus. The function of dsRBD domains in RNaseIII enzymes appears to be variable. The single dsRBD in *Aquifex aeolicus* RNaseIII was found to play a major role in substrate recognition.[8] In Dicer proteins, substrate binding is shared between the dsRBD and other domains with RNA binding capabilities.[9] In human Dicer, the dsRBD is located on the side of the active site cleft, suggesting its participation in dsRNA binding.[10] More recently, Ma et al. showed that the dsRBD in human Dicer participates in substrate binding together with the PAZ domain, but it is not essential for its activity or product length determination.[9] The dsRBD in *Schizosaccharomyces pombe* Dicer is not necessary for the RNase activity and has been shown to participate in the subcellular localization of the protein instead. This domain has a noncanonical structure showing a large $\beta1-\beta2$ loop and a Zn(II) binding site and was shown to bind both dsRNA and dsDNA.[11]

Arabidopsis thaliana has four related enzymes called Dicer-like ribonucleases (DCL1−4) that take part in small RNA metabolism, but only DCL1 participates in miRNA processing. A distinguishing feature of DCL1, -3, and -4 is the presence of a second dsRBD at the C-terminus (DCL1-B).[12] The exact role of this domain in the function of DCL proteins is hitherto unknown. This domain diverges in sequence from the first one, which is more closely related to the dsRBD in animal Dicer proteins, and was suggested to be a candidate for regulating substrate specificity and the interaction with associated proteins. There is experimental evidence supporting both roles. DCL1-B was shown to determine the accuracy of precursor processing in vivo.[13] This suggests that DCL1-B could specifically recognize the structure of the precursors ensuring the correct positioning of the processing complex to release the miRNA. On the other hand, DCL1-B was found to be essential for the localization of DCL1 at the proposed site of

Received: September 12, 2012
Revised: November 26, 2012
Published: November 29, 2012

miRNA processing in the nucleus, the dicing bodies.[14] However, no detailed characterization of this domain has been reported so far. With the aim of gaining insight into the function of DCL1-B in plant miRNA processing, we report here the solution structure and a functional characterization of the domain from *A. thaliana*.

EXPERIMENTAL PROCEDURES

Protein Expression and Purification. DCL1-B (detailed below) was amplified by polymerase chain reaction from a cDNA library and cloned into the pET-TEV expression vector.[15] The plasmid was transformed in *Escherichia coli* BL21(DE3) cells, which were then grown at 37 °C in M9 minimal medium supplemented with either 1 g/L $^{15}NH_4Cl$ or 1 g/L $^{15}NH_4Cl$ and 2 g/L [U-^{13}C]glucose (Cambridge Isotope Laboratories). Protein expression was induced at an OD_{600} of ≈0.7, and cells were grown overnight at 25 °C. The cells were harvested by centrifugation. Cell pellets were resuspended in 50 mM Tris (pH 8.0), 500 mM NaCl, 5 mM imidazole, and 1 mM β-mercaptoethanol and lysed by sonication. The clarified supernatant was purified using a Ni(II)-affinity column, and the protein was eluted with the same buffer supplemented with 350 mM imidazole. Fractions containing the protein were concentrated and digested with His-tagged TEV protease.[16] The protease was removed with a Ni(II)-affinity column, and the protein was further purified by an ion-exchange chromatography step on a CM-Sephadex column.

HYL1-dsRBD1−2 was produced and purified as described previously.[17]

RNA Synthesis. RNA samples were produced by in vitro transcription with T7 RNA polymerase, using annealed oligonucleotides. Briefly, a mix was prepared containing 1× transcription buffer [40 mM Tris (pH 8), 5 mM DTT, 1 mM spermidine, 0.01% Triton X-100, and 80 mg/mL PEG 8000], each rNTP at 4 mM (rA, rC, rG, and rU), 20 mM $MgCl_2$, 40 μg/mL BSA, and 1 unit of pyrophosphatase, and the annealed template at 35 μg/mL. The reaction was started by addition of T7 RNA polymerase and allowed to proceed for 3 h at 37 °C. Then, 50 units of RNase-free DNase was added, and the mix was incubated further for 30 min at 37 °C. The reaction mixture was then diluted 8-fold in 20 mM Tris, 10 mM EDTA, and 8 M urea (pH 8.0) and loaded on a Q-Sepharose column equilibrated with the same buffer. The column was eluted with a gradient from 0 to 1 M NaCl in the same buffer. Fractions containing RNA, as determined by A_{260}, were checked via denaturing 5% polyacrylamide gel electrophoresis. The fractions with the desired transcript were pooled, dialyzed three times against 200 volumes of H_2O, and lyophilized for storage before being used.

Fluorescence Anisotropy Titrations. For fluorescence anisotropy titrations, RNA fragments were labeled with fluorescein using the 5′ EndTag Nucleic Acid End Labeling System and fluorescein maleimide-thiol reactive label from Vector Laboratories. Labeled fragments were purified by phenol extraction, precipitated with ethanol, and resuspended on 10 mM phosphate buffer (pH 7.0). Fluorescein-labeled DNA was obtained from Sigma. The fluorescence anisotropy was measured on a Varian Cary Eclipse spectrofluorimeter exciting the sample at 492 nm and measuring emission at 520 nm. Anisotropy values were obtained from the average of three measurements with an integration time of 20 s. The excitation and emission slits were set to 10 nm. Labeled RNA was annealed by being heated at 100 °C for 5 min and chilled in an ice/water bath, to ensure correct intramolecular hybridization. Labeled DNA oligomers were annealed by being mixed together, heated at 100 °C, and slowly cooled to room temperature. The buffer of each protein sample was exchanged with 10 mM phosphate (pH 7.0) immediately before the titrations were performed by employing micro Bio-Spin 6 columns (Bio-Rad) according to the manufacturer's instructions. Binding curves were constructed at 20 °C titrating a 50 nM solution of labeled nucleic acid, in 10 mM phosphate buffer (pH 7.0), with increasing concentrations of the corresponding protein. Experimental data points (r) were fit to a either a hyperbolic function (eq 1), on the assumption of a simple binding model with a 1:1 stoichiometry, or a Hill equation (eq 2):

$$r = r_0 + (a[\mathrm{P}])/(b + [\mathrm{P}]) \quad (1)$$

$$r = r_0 + (a[\mathrm{P}]^n)/(b^n + [\mathrm{P}]^n) \quad (2)$$

where [P] corresponds to free protein concentration, r_0 is the anisotropy of free RNA (or DNA), a is the amplitude of the change in anisotropy upon binding, b is the dissociation constant, and n is the Hill coefficient, which gives a measure of the binding cooperativity for systems with a binding stoichiometry of >1:1. Titration curves were normalized for plotting by subtracting from each data point the value of r_0 and dividing the result by amplitude a.

Nuclear Magnetic Resonance (NMR) Spectroscopy. NMR spectra were recorded at 298 K. All spectra were processed with NMRPipe and analyzed with NMRView or CCPNMR. Chemical shifts were referenced with respect to the H_2O signal at 4.77 ppm (pH 6.8, 25 °C) relative to DSS, using the ^{1}H:X frequency ratios of the zero point according to Markley et al.[18] Backbone ^{1}H, ^{13}C, and ^{15}N chemical shifts of DCL1-B were assigned using a set of triple-resonance spectra [BEST-HNCA/HN(CO)CA, BEST-HNCACB/HN(CO)CACB, BEST-HN(CA)CO/HNCO, and HN(CA)HA][19] collected on a 600 MHz Bruker spectrometer. The side chain resonances were assigned with H(CC)(CO)NH and (H)CCH-TOCSY spectra, and the assignment was completed by analyzing ^{15}N- and ^{13}C-edited NOESY spectra. Aromatic proton resonances were assigned using ^{1}H−^{1}H NOESY and ^{1}H−^{1}H TOCSY in ^2H_2O. The complete assignment was deposited in the BioMagResBank (entry 18393).

Distance restraints were derived from three-dimensional ^{15}N- and ^{13}C-edited NOESY spectra and two-dimensional (2D) ^{1}H−^{1}H NOESY spectra (t_m = 120 ms) collected on an 800 MHz VNMRS Varian spectrometer equipped with a triple-resonance (^{1}H, ^{13}C, ^{15}N) cryoprobe. For acquisition of RDC data, DCL1-B was aligned in a 5% C12E5/hexanol (C12E5:hexanol ratio of 0.96) liquid crystalline phase.[20] RDC values were measured for three atom pairs on each peptide plane (D_{N-HN}, $D_{C'-HN}$, and $D_{C'-N}$) from C′-coupled ^{15}N IPAP-HSQC spectra.[21]

Protein−RNA/DNA and protein−protein interaction experiments were conducted at 298 K on a 600 MHz Bruker NMR spectrometer equipped with an Avance II console and a TXI-Z probe. RNA/DNA titrations were conducted in 50 mM Hepes (pH 7.0), 10 mM DTT, 0.05% azide, 1× Complete, and 10% D_2O. The pre-miR172 lower-stem fragment was annealed by being heated to 100 °C and flash-cooled in an ice/water bath. Titrations were performed by addition of nucleic acid to a 100 μM protein sample. At each step, a ^{1}H−^{15}N SOFAST-HMQC spectrum[22] was acquired. The interaction of DCL1-B with

Table 1. Statistics for the 20 Final Structures of DCL1-dsRBD2

no. of distance restraints	
unambiguous restraints	960
intraresidual	428
sequential	212
short range	110
medium range	18
long range	192
ambiguous restraints	179
dihedral angles restraints	108 (52 φ, 52 ψ)
RDCs	
no. of RDC restraints	112 (56 HN−N, 56 HN−C′)
tensor **Aa**	8.34×10^{-4}
tensor **Ar**	2.64×10^{-4}
χ^2	560.7
Q factor	0.215
violations	
distance	
root-mean-square deviation (rmsd)	0.032 Å
largest	0.45 Å
dihedrals	
rmsd	0.87°
largest	9.57°
mean deviation from ideal covalent geometry	
bond lengths	0.004 Å
bond angles	0.572°
rmsd with respect to mean structure (residues 16−32, 42−83)	
backbone	0.29 ± 0.07 Å
heavy atoms	0.80 ± 0.10 Å
CING ROG analysis (residues 16−32, 42−83)	
red	12 (20%)
orange	16 (27%)
green	31 (53%)
Ramachandran analysis (residues 16−32, 42−83)	
core	91.4%
allowed	8.6%
generous and disallowed	0.0%

HYL1-dsRBD1−2 was evaluated by addition of 1 equiv of unlabeled HYL1-dsRBD1−2 to ^{15}N-labeled DCL1-B in 100 mM phosphate, 50 mM NaCl, and 1 mM β-mercaptoethanol (pH 7.0). A ^{1}H−^{15}N HSQC spectrum was acquired for free DCL1-B and another for the 1:1 mix of DCL1-B and HYL1-dsRBD1−2. The final concentration for both proteins was 110 μM.

Structure Calculation. The structure was calculated on the basis of the distance restraints obtained from NOESY experiments and D_{N-HN} and $D_{C'-HN}$ residual dipolar couplings. Cross-peaks from the ^{15}N- and ^{13}C-edited NOESY spectra were automatically picked and assigned using the ATNOS-CANDID algorithm[23,24] implemented in UNIO'10. The aromatic region of the ^{1}H−^{1}H 2D NOESY spectrum was picked manually, and peak picking of the ^{15}N NOESY spectrum was completed by hand. Torsion ϕ and ψ angles calculated from the H, N, CA, CB, HA, and CO chemical shift values using the online version of TALOS+[25] were used as additional restraints. Structures were calculated using ARIA 2.3.1/CNS 1.1,[26,27] allowing for reassignment of the peak lists initially provided by UNIO'10. The axial and rhombic components of the alignment tensor were determined with Pales[28] by best fitting the experimental residual dipolar couplings to the lowest-energy conformer of the preceding structure calculation. The following expressions were used as described previously:[28] $D = (\mu_0/8\pi^3)h\gamma_i\gamma_j(r_{ij})^{-3} \times$ Da and r = Dr/Da. One thousand structures were calculated in the last Aria iteration, from which 20 conformers with the lowest total energy were submitted to water refinement.

RESULTS

Structure Calculation. To study the structure of DCL1-B, we generated a protein construct spanning the domain as defined on the DCL1 sequence by prosite (http://prosite.expasy.org/), including five extra residues to the N-terminal side. The construct included residues N1826−S1909. We expressed the construct labeled with ^{15}N and found that it has a well-dispersed ^{1}H−^{15}N HSQC spectrum, indicating that it can fold independently of the rest of the protein. Sequential resonance assignments and structural constraints were obtained from a series of NMR experiments on uniformly ^{15}N-labeled and ^{13}C- and ^{15}N-labeled samples. The structures were calculated with ARIA-CNS using NOE-derived distance restraints, Talos+-derived torsion angle restraints, and HN−N and HN−C′ residual dipolar couplings. The calculated structures include residues N1837−T1907 within our construct, as only few weak resonances could be identified outside this region. The statistics for the calculated structures are listed

dx.doi.org/10.1021/bi301247r | *Biochemistry* 2012, 51, 10159−10166

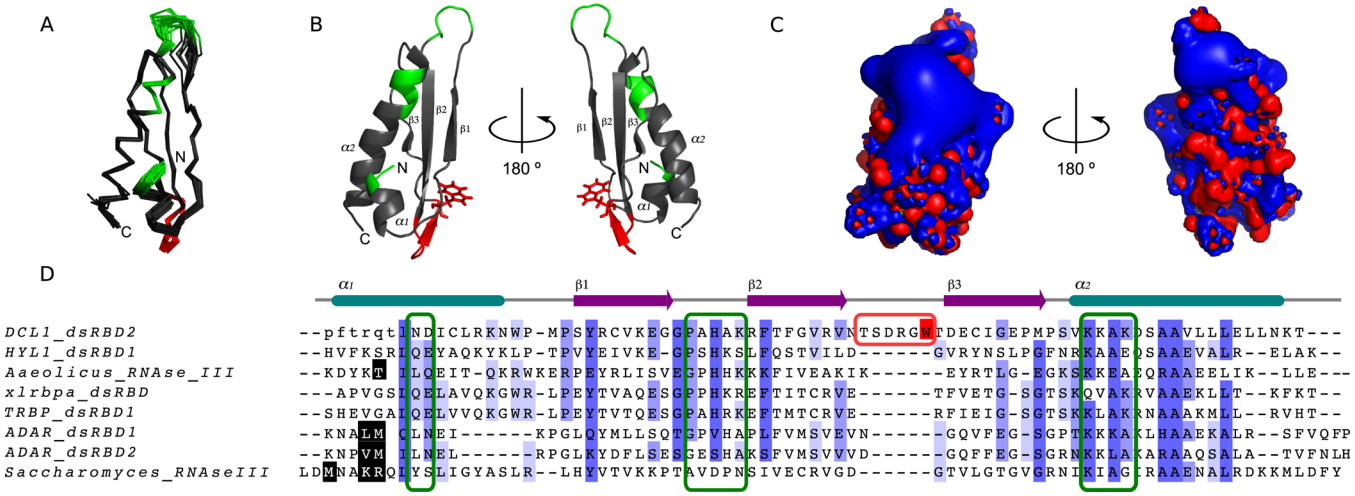

Figure 1. (A) Ribbon representation of the bundle of the 20 lowest-energy structures obtained from the solution structure calculation. (B) Solution structure of DCL1-B. Putative RNA binding regions, as inferred from sequence alignment, are colored green. The insertion between β2 and β3 is colored red. The side chain of tryptophan 1877 is shown as sticks. (C) Electrostatic potential of the domain. Isosurfaces at 3.5 V (blue) and −3.5 V (red) are shown. The orientation of the domain is the same as in panel B. A large positive potential region is observed over the putative RNA binding regions. (D) Alignment of the sequence of DCL1-B with the sequences of dsRBDs for which structures in complex with RNA are available. The residues at the N-terminus of DCL1-B not observed in the ^{1}H−^{15}N HSQC spectrum are shown in lowercase letters. The secondary structure elements are indicated at the top of the alignment. Residues are highlighted in blue shades according to the degree of sequence conservation. Green boxes highlight the three RNA interaction motifs. Residues in helix 1 that participate in dsRNA binding are shown on a black background. The red box highlights the insertion in DCL1-B. Trp1877 is shown on a red background.

in Table 1. The structure was deposited in the Protein Data Bank (entry 2LRS).

The topology of the protein corresponds to that of a regular dsRBD, namely $\alpha/\beta/\beta/\beta/\alpha$ (Figure 1). Binding of dsRNA by these domains is mediated by three regions: helix α1 (motif 1), the loop between strands β1 and β2 (motif 2), and the N-terminal end of helix α2 (motif 3).[29] The structure of residues belonging to motifs 2 and 3 is well-conserved in our structure. However, helix α1, bearing residues corresponding to motif 1, appears to be shorter than in canonical dsRBDs, as the absence of most main chain amide resonances for residues preceding N1837 suggests that this region does not adopt a well-defined structure. The low values of ^{1}H−^{15}N NOEs for the few signals corresponding to residues N1826−N1837 present in the spectrum further support a higher mobility in this region (Figure 2). Shortening of helix 1 may have a direct implication on dsRNA binding by DCL1-B, as this region plays a major role in the recognition of the dsRNA structure[30−34] (Figure 1 and Figure 1 of the Supporting Information). This flexible region could confer upon DCL1-B the versatility to recognize pre-miRNA molecules with heterogeneous secondary and tertiary structures as well as dsDNA (see below).

Another interesting feature in the structure of DCL1-B is the presence of a six-residue insertion between strands β2 and β3. This insertion is located on the opposite side of the expected RNA-binding interface in DCL1-B and should not alter the affinity and specificity for nucleic acids, or at least not in a direct way. Heteronuclear NOE data suggest that this region is not flexible, showing only slightly lower than average ^{1}H−^{15}N NOEs (Figure 2). Within the insertion, the methyl groups of Thr1872 and Thr1878 are part of a hydrophobic pocket, which hosts the side chain of Trp1845, located in the loop between helix α1 and strand β2. The presence of an aromatic residue in this position was shown to confer stability to the dsRBD fold.[35] This extended loop could help in this way to stabilize the fold of DCL1-B. It is also noteworthy that the side chain of

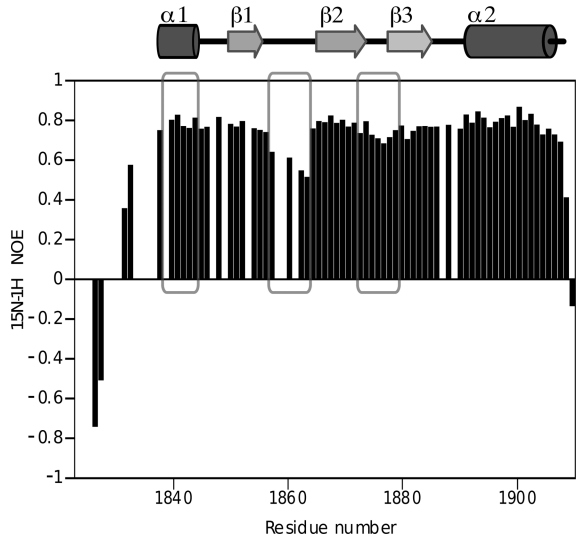

Figure 2. Heteronuclear (^{1}H−^{15}N) NOEs for DCL1-B. The secondary structure elements are indicated at the top. Boxed regions correspond (in order) to helix 1, the loop between strand 1 and 2 (RNA binding motif 2), and the insertion between strands β2 and β3.

Trp1877, located within the insertion, protrudes from the face opposite the putative RNA-binding surface. This Trp residue is fully conserved among DCL1-B domains from different plants but is not present in the sequences of the DCL3-B or DCL4-B domain (Figure 2 of the Supporting Information). The presence of a bulky aromatic residue on the surface of the protein can indicate a protein−protein interaction surface,[36] which could be important for the function of DCL1 in the context of the miRNA processing complex.

The C-terminal dsRBDs of DCL1 were reported to interact with the dsRBDs of HYL1.[37] We decided to investigate whether DCL1-B participated in this interaction in vitro, by titrating ^{15}N-labeled DCL1-B with unlabeled HYL1-dsRBD1−

dx.doi.org/10.1021/bi301247r | Biochemistry 2012, 51, 10159−10166

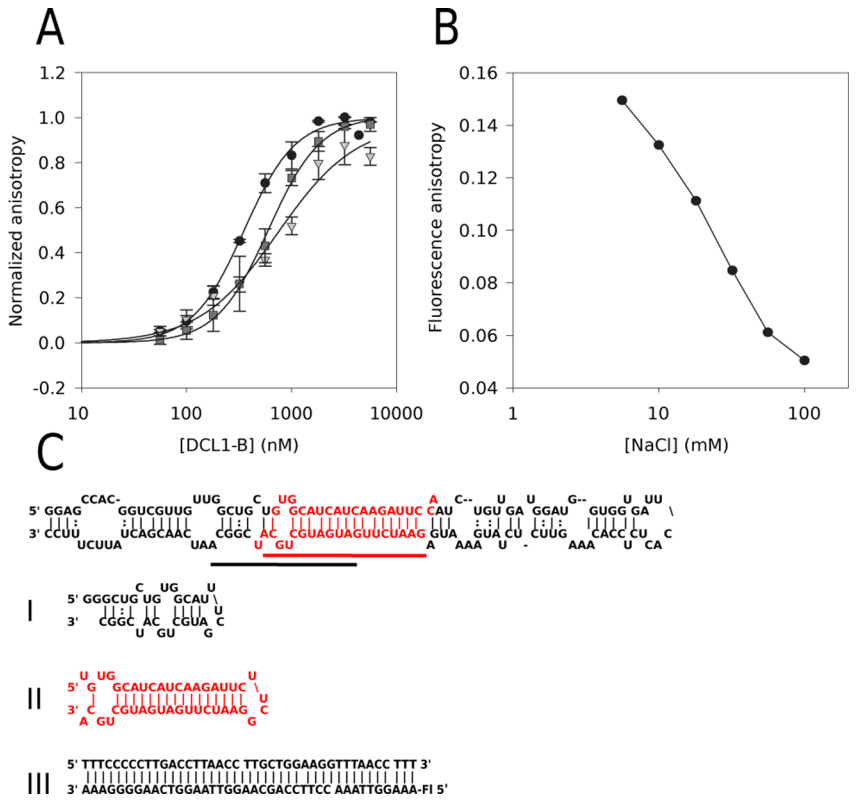

Figure 3. Interaction of DCL1-B with dsRNA and dsDNA followed by fluorescence anisotropy. (A) Titration of fluorescently labeled nucleic acids with DCL1-B. Data points correspond to the average of three (miR172-lower stem, circles) or two (mir172, triangles; dsDNA, squares) independent experiments; error bars denote the standard error. Estimated dissociation constants were 350 ± 20, 810 ± 180, and 600 ± 50 nM for miR172-lower stem, miR172, and dsDNA, respectively. The data for miR172-lower stem and dsDNA were fit to a Hill equation (Hill coefficient of 1.8 in both cases). (B) Ionic strength dependence of dsRNA binding by DCL1-B. Increasing amounts of NaCl were added to a solution of 50 nM fluorescein-labeled miR172-lower stem RNA and 3.2 μM DCL1-B. Reduction of the fluorescence anisotropy indicates the dissociation of the complex at higher ionic strengths. The abscissas are plotted on a logarithmic scale. (C) Nucleic acid constructs used. The secondary structure of pri-miR172 is shown at the top, and the miRNA/miRNA* is highlighted in red. Construct I corresponds to the lower-stem region. Construct II corresponds to the miRNA region. Construct III is the double-stranded DNA sequence. Fl indicates the fluorescein label.

2. The $^{1}H-^{15}N$ HSQC spectra of DCL1-B did not show any significant change upon addition of HYL1-dsRBDs (Figure 3 of the Supporting Information), indicating that HYL1 dsRBDs do not interact with DCL1-B, or at least not in a direct way.

RNA Binding. To investigate RNA recognition by DCL1-B, we performed fluorescence anisotropy measurements. We studied the interaction of the protein construct with fragments of the miR172a precursor (pri-miR172a) corresponding to the miRNA/miRNA* and to the lower-stem (pre-miRNAls) regions (Figure 3). The lower-stem region was recently shown to be essential in defining the register for pri-miRNA processing in plants[5] and is less structured than the miRNA region. The affinity of DCL1-B for both constructs is similar ($K_{D,lower\text{-}stem}$ = 350 ± 20 nM; $K_{D,miRNA/miRNA*}$ = 810 ± 180 nM), indicating that the domain is not likely to recognize particular features in the precursor structure. The slightly higher affinity for the lower-stem region suggests that DCL1-B has some preference for imperfect double-stranded RNA (Figure 3). Increasing the ionic strength of the buffer solution diminishes the strength of the interaction, evidencing that binding of RNA is largely mediated by an electrostatic component (Figure 3). Calculation of the electrostatic potential of DCL1-B shows a large positive potential on the RNA-binding region of the protein, further supporting this observation.

As a control, we also tested binding of DCL1-B to double-stranded DNA using the same kind of assay. We were surprised to verify that it does bind dsDNA with an affinity similar to that of precursor RNA ($K_{D,dsDNA}$ = 600 ± 50 nM). In a control experiment with HYL1-dsRBD1, a canonical dsRBD, we found a large difference in affinity between dsRNA and dsDNA (Figure 4 of the Supporting Information). Binding of dsDNA with high affinity is a rather unusual feature for dsRBDs, which are known for their ability to discriminate between different types of nucleic acids (ss- and dsRNA vs ss- and dsDNA). The dual specificity may come as a result of the dynamic nature of the residues preceding the short helix 1 in DCL1-B and the largely electrostatic nature of the protein−nucleic acid interaction.

To improve our understanding of the determinants of the recognition of nucleic acids by this domain, we mapped the interaction regions by titrating the pre-miR172 lower-stem construct and dsDNA on ^{15}N-labeled protein samples, following the changes in $^{1}H-^{15}N$ HSQC spectra. When titrating the RNA construct on DCL1-B, we found that many signals decay in intensity, even at very low (1:100) RNA:protein ratios, without any major change in chemical shifts. At the same time, the imino ^{1}H signals from the RNA are clearly visible, showing that the decrease in the intensity of the protein signals is not due to the formation of large complexes or aggregates, which would lead to broadening of the signals beyond detection. The observed behavior thus suggests that the protein in the complex is in an intermediate-exchange regime

dx.doi.org/10.1021/bi301247r | *Biochemistry* 2012, 51, 10159−10166

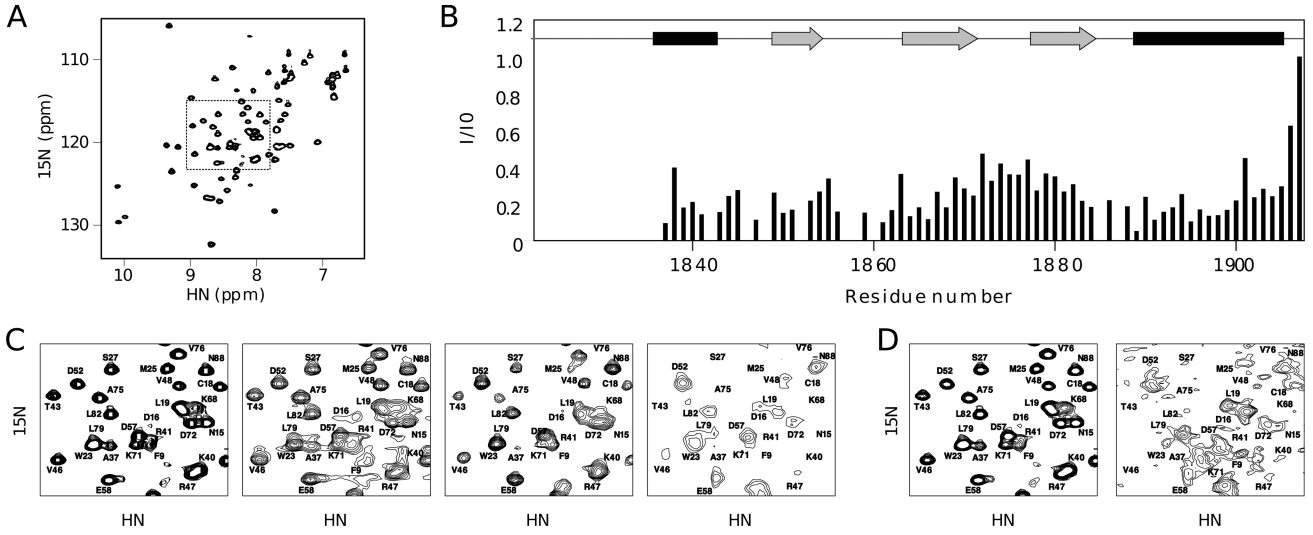

Figure 4. NMR characterization of the interaction between DCL1-B and nucleic acids. (A) Spectrum of free DCL1-B. The dashed rectangle shows the region magnified in panels C and D. (B) Intensity ratios vs sequence for the spectra of free DCL1-B in the presence of 0.05 equiv of pre-miR172 lower stem. (C) Titration of DCL1-B with RNA followed by NMR. The spectra correspond to (from left to right) free protein and 0.01, 0.05, and 0.1 equiv of pre-miR172 lower stem, respectively. (D) NMR spectrum of free DCL1-B and DCL1-B in the presence of 0.05 equiv of dsDNA.

and that it binds the RNA adopting multiple conformations. Although the spectra show a generalized decrease in intensity, even at low RNA:protein ratios, the analysis of the signal intensity profile shows that the $\beta2-\beta3$ loop and the C-terminus of helix $\alpha2$ are less affected than the rest of the protein (Figure 4B and Figure 5 of the Supporting Information). The less affected regions are located opposite the putative RNA binding motifs in the structure, thus suggesting that DCL1-B binds RNA in a manner similar to that of canonical dsRBDs. Titrating the protein with dsDNA leads to a similar behavior (Figure 4 and Figure 6 of the Supporting Information). We therefore conclude that DCL1-B forms heterogeneous complexes with the tested dsRNA and dsDNA substrates, which are in an intermediate-exchange regime.

■ DISCUSSION

DCL1-B is essential for the correct function of the protein. Truncation of DCL1 at this site (*dcl1–9* mutant) leads to a general decrease in miRNA levels and phenotypic abnormalities.[38] It has been suggested that the second dsRBD in DCL1 was necessary for precursor structure recognition and for the correct location of the RNase III active sites within the precursor. If this were the case, we would expect DCL1-B to recognize and bind to some particular feature of the precursors. We found that DCL1-B does bind to precursor RNA, but with no specificity, as inferred from the NMR spectra and the similar binding affinities of the domain for different regions in the precursor and dsDNA. Therefore, we hypothesize that this domain must have functions other than the location of the miRNA position within the precursor.

A defining feature of dsRBDs is the ability to discriminate between dsRNA and dsDNA, DNA–RNA hybrids, or single-stranded nucleic acids.[39−42] However, we found that DCL1-B binds dsRNA and dsDNA with similar affinities. The structures of canonical dsRBD–dsRNA complexes determined to date have shown that the discrimination against dsDNA can be explained by specific interactions of the protein with the phosphate groups in the backbone and with 2′-OH groups in the ribose moieties.[30−33,43] In particular, most specific contacts involve helix $\alpha1$ [a conserved L(Q/N)(E/D) motif] and the $\beta1-\beta2$ loop (a conserved His residue in the center of the loop). The separation between these regions corresponds to the groove dimensions of A-form double-stranded nucleic acids, further adding to the discrimination.[34] It was recently reported that the noncanonical dsRBD of fission yeast Dicer does bind to dsDNA as well.[11] In this case, the domain has an unusually long loop between strands 1 and 2 and a different position of helix $\alpha1$, which can explain the dual binding capacity. Our structural analysis of DCL1-B shows a short structured helix $\alpha1$ and a dynamic nature for the residues preceding it. These features could account for the ability to bind both dsRNA and dsDNA. The conformational flexibility of the region preceding the short helix 1, which could be involved in interactions with the nucleic acid partner, would cause the heterogeneity observed in the DCL1-B–dsRNA and DCL1-B–dsDNA complexes as well.

It has been shown that the truncated DCL1–9 protein fails to localize to the dicing bodies in the nucleus, thus revealing a role for DCL1-B in defining the subcellular localization of DCL1.[14] In a similar fashion, the noncanonical dsRBD of fission yeast Dicer was shown to mediate the localization of the protein.[11] A possible mechanism for this function would be the specific interaction with other proteins in the nucleus. It was reported that HYL1 dsRBDs interact with the C-terminal dsRBDs of DCL1,[37] but we could not detect the reported interaction in vitro (Figure 3 of the Supporting Information). However, several other proteins have been shown to participate in plant miRNA processing that could be potential partners for DCL1-B.[7] It is then possible that DCL1-B has evolved to determine DCL1 localization through specific protein–protein interactions, leaving nucleic acid binding as a vestigial feature of the protein. The insertion between strands $\beta2$ and $\beta3$, which includes an exposed tryptophan side chain, could represent a potential protein–protein interaction surface.

In summary, we obtained the solution structure of DCL1-B and showed that it has a canonical fold with some variations that can be functionally relevant. We found that this domain binds precursor RNA with no preference for different regions of

the substrate and that it can also bind dsDNA. In light of the available biological information and sequence analysis, our results suggest that this domain, showing features not seen in other dsRBDs, likely has functions beyond substrate recognition and binding.

■ ASSOCIATED CONTENT

Supporting Information

Supplementary Figures 1−6. This material is available free of charge via the Internet at http://pubs.acs.org.

■ AUTHOR INFORMATION

Corresponding Author

*E-mail: rasia@ibr.gov.ar. Phone: +54 341 4237070, ext. 615.

Present Address

⊥Swiss Federal Institute of Technology (ETH), 8092 Zurich, Switzerland.

Funding

This work was supported by Grant PICT 2007 720 from ANPCyT to R.M.R., a 2009 cooperation grant from CONICET and CNRS to J.F.P. and Dr. Jèrôme Boisbouvier (IBS-Grenoble) and the TGIR-RMN-THC Fr3050. P.B. is recipient of a fellowship from ANPCyT. I.P.S. is recipient of a fellowship from CONICET. J.F.P. and R.M.R. are members of CONICET.

Notes

The authors declare no competing financial interest.

■ ACKNOWLEDGMENTS

The authors thank the Grenoble Partnership for Structural Biology for access to integrated structural biology Cell-Free platform, Lionel Imbert for help with the synthesis of RNA samples and Dr. Jèrôme Boisbouvier for helpful discussions.

■ ABBREVIATIONS

dsRBD, dsRNA binding domain; DCL, Dicer-like protein.

■ REFERENCES

(1) Filipowicz, W., Bhattacharyya, S. N., and Sonenberg, N. (2008) Mechanisms of post-transcriptional regulation by microRNAs: Are the answers in sight? *Nat. Rev. Genet. 9*, 102−114.

(2) Han, J., Lee, Y., Yeom, K.-H., Nam, J.-W., Heo, I., Rhee, J.-K., Sohn, S. Y., Cho, Y., Zhang, B.-T., and Kim, V. N. (2006) Molecular basis for the recognition of primary microRNAs by the Drosha-DGCR8 complex. *Cell 125*, 887−901.

(3) Song, L., Axtell, M. J., and Fedoroff, N. V. (2010) RNA secondary structural determinants of miRNA precursor processing in *Arabidopsis*. *Curr. Biol. 20*, 37−41.

(4) Werner, S., Wollmann, H., Schneeberger, K., and Weigel, D. (2010) Structure determinants for accurate processing of miR172a in *Arabidopsis thaliana*. *Curr. Biol. 20*, 42−48.

(5) Mateos, J. L., Bologna, N. G., Chorostecki, U., and Palatnik, J. F. (2010) Identification of MicroRNA processing determinants by random mutagenesis of *Arabidopsis* MIR172a precursor. *Curr. Biol. 20*, 49−54.

(6) Dong, Z., Han, M.-H., and Fedoroff, N. (2008) The RNA-binding proteins HYL1 and SE promote accurate in vitro processing of pri-miRNA by DCL1. *Proc. Natl. Acad. Sci. U.S.A. 105*, 9970−9975.

(7) Xie, Z., Khanna, K., and Ruan, S. (2010) Expression of microRNAs and its regulation in plants. *Semin. Cell Dev. Biol. 21*, 790−797.

(8) Gan, J., Tropea, J. E., Austin, B. P., Court, D. L., Waugh, D. S., and Ji, X. (2006) Structural Insight into the Mechanism of Double-Stranded RNA Processing by Ribonuclease III. *Cell 124*, 355−366.

(9) Ma, E., Zhou, K., Kidwell, M. A., and Doudna, J. A. (2012) Coordinated Activities of Human Dicer Domains in Regulatory RNA Processing. *J. Mol. Biol. 422*, 466−476.

(10) Lau, P.-W., Guiley, K. Z., De, N., Potter, C. S., Carragher, B., and MacRae, I. J. (2012) The molecular architecture of human Dicer. *Nat. Struct. Mol. Biol. 19*, 436−440.

(11) Barraud, P., Emmerth, S., Shimada, Y., Hotz, H.-R., Allain, F. H.-T., and Buhler, M. (2011) An extended dsRBD with a novel zinc-binding motif mediates nuclear retention of fission yeast Dicer. *EMBO J. 30*, 4223−4235.

(12) Margis, R., Fusaro, A. F., Smith, N. A., Curtin, S. J., Watson, J. M., Finnegan, E. J., and Waterhouse, P. M. (2006) The evolution and diversification of Dicers in plants. *FEBS Lett. 580*, 2442−2450.

(13) Kurihara, Y., and Watanabe, Y. (2004) *Arabidopsis* micro-RNA biogenesis through Dicer-like 1 protein functions. *Proc. Natl. Acad. Sci. U.S.A. 101*, 12753−12758.

(14) Fang, Y., and Spector, D. L. (2007) Identification of nuclear dicing bodies containing proteins for microRNA biogenesis in living *Arabidopsis* plants. *Curr. Biol. 17*, 818−823.

(15) Houben, K., Marion, D., Tarbouriech, N., Ruigrok, R. W. H., and Blanchard, L. (2007) Interaction of the C-terminal domains of sendai virus N and P proteins: Comparison of polymerase-nucleocapsid interactions within the paramyxovirus family. *J. Virol. 81*, 6807−6816.

(16) Kapust, R. B., Tözsér, J., Fox, J. D., Anderson, D. E., Cherry, S., Copeland, T. D., and Waugh, D. S. (2001) Tobacco etch virus protease: Mechanism of autolysis and rational design of stable mutants with wild-type catalytic proficiency. *Protein Eng. 14*, 993−1000.

(17) Rasia, R. M., Mateos, J. L., Bologna, N. G., Burdisso, P., Imbert, L., Palatnik, J. F., and Boisbouvier, J. (2010) Structure and RNA interactions of the plant microRNA processing-associated protein HYL1. *Biochemistry 49*, 8237−8239.

(18) Markley, J. L., Bax, A., Arata, Y., Hilbers, C. W., Kaptein, R., Sykes, B. D., Wright, P. E., and Wüthrich, K. (1998) Recommendations for the presentation of NMR structures of proteins and nucleic acids: IUPAC-IUBMB-IUPAB Inter-Union Task Group on the standardization of data bases of protein and nucleic acid structures determined by NMR spectroscopy. *Eur. J. Biochem. 256*, 1−15.

(19) Lescop, E., Schanda, P., and Brutscher, B. (2007) A set of BEST triple-resonance experiments for time-optimized protein resonance assignment. *J. Magn. Reson. 187*, 163−169.

(20) Rückert, M., and Otting, G. (2000) Alignment of Biological Macromolecules in Novel Nonionic Liquid Crystalline Media for NMR Experiments. *J. Am. Chem. Soc. 122*, 7793−7797.

(21) Wang, Y.-X., Marquardt, J. L., Wingfield, P., Stahl, S. J., Lee-Huang, S., Torchia, D., and Bax, A. (1998) Simultaneous Measurement of $^{1}H-^{15}N$, $^{1}H-^{13}C'$, and $^{15}N-^{13}C'$ Dipolar Couplings in a Perdeuterated 30 kDa Protein Dissolved in a Dilute Liquid Crystalline Phase. *J. Am. Chem. Soc. 120*, 7385−7386.

(22) Schanda, P., and Brutscher, B. (2005) Very fast two-dimensional NMR spectroscopy for real-time investigation of dynamic events in proteins on the time scale of seconds. *J. Am. Chem. Soc. 127*, 8014−8015.

(23) Herrmann, T., Güntert, P., and Wüthrich, K. (2002) Protein NMR Structure Determination with Automated NOE Assignment Using the New Software CANDID and the Torsion Angle Dynamics Algorithm DYANA. *J. Mol. Biol. 319*, 209−227.

(24) Herrmann, T. (2010) Protein Structure Calculation and Automated NOE Restraints. In *Encyclopedia of Magnetic Resonance*, Wiley, New York.

(25) Shen, Y., Delaglio, F., Cornilescu, G., and Bax, A. (2009) TALOS+: A hybrid method for predicting protein backbone torsion angles from NMR chemical shifts. *J. Biomol. NMR 44*, 213−223.

(26) Downing, A. K., and Güntert, P. (2004) Automated NMR Structure Calculation with CYANA. *Methods Mol. Biol.*, 353−378.

(27) Rieping, W., Habeck, M., Bardiaux, B., Bernard, A., Malliavin, T. E., and Nilges, M. (2007) ARIA2: Automated NOE assignment and data integration in NMR structure calculation. *Bioinformatics 23*, 381−382.

(28) Zweckstetter, M. (2008) NMR: Prediction of molecular alignment from structure using the PALES software. *Nat. Protoc. 3*, 679−690.
(29) Masliah, G., Barraud, P., and Allain, F. (2012) RNA recognition by double-stranded RNA binding domains: A matter of shape and sequence. *Cell. Mol. Life Sci.*, in press.
(30) Ryter, J. M., and Schultz, S. C. (1998) Molecular basis of double-stranded RNA-protein interactions: Structure of a dsRNA-binding domain complexed with dsRNA. *EMBO J. 17*, 7505−7513.
(31) Ramos, A., Grünert, S., Adams, J., Micklem, D. R., Proctor, M. R., Freund, S., Bycroft, M., St Johnston, D., and Varani, G. (2000) RNA recognition by a Staufen double-stranded RNA-binding domain. *EMBO J. 19*, 997−1009.
(32) Blaszczyk, J., Gan, J., Tropea, J. E., Court, D. L., Waugh, D. S., and Ji, X. (2004) Noncatalytic assembly of ribonuclease III with double-stranded RNA. *Structure 12*, 457−466.
(33) Stefl, R., Oberstrass, F. C., Hood, J. L., Jourdan, M., Zimmermann, M., Skrisovska, L., Maris, C., Peng, L., Hofr, C., Emeson, R. B., and Allain, F. H.-T. (2010) The Solution Structure of the ADAR2 dsRBM-RNA Complex Reveals a Sequence-Specific Readout of the Minor Groove. *Cell 143*, 225−237.
(34) Tian, B., Bevilacqua, P. C., Diegelman-Parente, A., and Mathews, M. B. (2004) The double-stranded-RNA-binding motif: Interference and much more. *Nat. Rev. Mol. Cell Biol. 5*, 1013−1023.
(35) Yamashita, S., Nagata, T., Kawazoe, M., Takemoto, C., Kigawa, T., Güntert, P., Kobayashi, N., Terada, T., Shirouzu, M., Wakiyama, M., Muto, Y., and Yokoyama, S. (2011) Structures of the first and second double-stranded RNA-binding domains of human TAR RNA-binding protein. *Protein Sci. 20*, 118−130.
(36) Bogan, A. A., and Thorn, K. S. (1998) Anatomy of hot spots in protein interfaces. *J. Mol. Biol. 280*, 1−9.
(37) Hiraguri, A., Itoh, R., Kondo, N., Nomura, Y., Aizawa, D., Murai, Y., Koiwa, H., Seki, M., Shinozaki, K., and Fukuhara, T. (2005) Specific interactions between Dicer-like proteins and HYL1/DRB-family dsRNA-binding proteins in *Arabidopsis thaliana*. *Plant Mol. Biol. 57*, 173−188.
(38) Jacobsen, S. E., Running, M. P., and Meyerowitz, E. M. (1999) Disruption of an RNA helicase/RNAse III gene in *Arabidopsis* causes unregulated cell division in floral meristems. *Development 126*, 5231−5243.
(39) St Johnston, D., Brown, N. H., Gall, J. G., and Jantsch, M. (1992) A conserved double-stranded RNA-binding domain. *Proc. Natl. Acad. Sci. U.S.A. 89*, 10979−10983.
(40) Bass, B. L., Hurst, S. R., and Singer, J. D. (1994) Binding properties of newly identified *Xenopus* proteins containing dsRNA-binding motifs. *Curr. Biol. 4*, 301−314.
(41) Bevilacqua, P. C., and Cech, T. R. (1996) Minor-Groove Recognition of Double-Stranded RNA by the Double-Stranded RNA-Binding Domain from the RNA-Activated Protein Kinase PKR. *Biochemistry 35*, 9983−9994.
(42) Lu, C., and Fedoroff, N. (2000) A mutation in the *Arabidopsis* HYL1 gene encoding a dsRNA binding protein affects responses to abscisic acid, auxin, and cytokinin. *Plant Cell 12*, 2351−2366.
(43) Yang, S. W., Chen, H.-Y., Yang, J., Machida, S., Chua, N.-H., and Yuan, Y. A. (2010) Structure of *Arabidopsis* HYPONASTIC LEAVES1 and Its Molecular Implications for miRNA Processing. *Structure 18*, 594−605.